Short-Packet Communications in Wireless Energy Transfer Full-Duplex IoT Networks with Deep Learning Design

Toan-Van Nguyen, Thien Huynh-The, and Vo-Nguyen Quoc Bao

***Abstract*—In this paper, we study wireless energy transfer full-duplex (FD) Internet-of-things (IoT) networks, where multiple FD IoT relays are deployed to assist short-packet communications between a source and a robot destination with multiple antennas in automation factories. Considering two residual interference (RSI) models for FD relays, we propose a full relay selection (FRS) scheme to maximize the e2e signal-to-noise ratio of packet transmissions. We derive the closed-form expressions for the average block error rate (BLER) and throughput of the considered system, based on which the approximation analysis is also carried out. Towards real-time configurations, we design a deep learning framework based on the FRS scheme to accurately predict the average BLER and system throughput via a short inference process. Simulation results reveal the significant effects of RSI models on the performance of FD IoT networks. Furthermore, the CNN design achieves the lowest root-mean-squared error among other schemes such as the conventional CNN and deep neural network. Furthermore, the DL framework can estimate similar BLER and throughput values as the FRS scheme, but with significantly reduced complexity and execution time, showing the potential of DL design in dealing with complex scenarios of heterogeneous IoT networks.**

***Index Terms*—Deep neural network, residual self-interference, short-packet communication, wireless power transfer.**

I. Introduction

SHORT-packet communication (SPC) has gained significant attention due to its potential applications in critical scenarios with stringent latency requirements such as autonomous driving, remote surgery, and factory automation [2], [3]. For the Internet-of-things (IoT) systems and wireless networks, SPC was considered to achieve low transmission latency, and high reliability with a small block error rate (BLER) [4], [5]. Recent studies in SPC with finite blocklength codes have primarily focused on the analysis of IoT systems with half-duplex (HD) transmissions, where strict requirements of 99.999% reliability and 1 ms latency demand utmost consideration [6].

Deep learning (DL) has recently emerged as a powerful solution to tackle a variety of practical problems in contemporary wireless IoT systems, including resource allocation, queue management, and congestion control [7]. By precisely estimating functions with high nonlinearity at a minimum of complexity, DL has been increasingly applied in wireless networks to improve various aspects of systems including resource allocation, throughput prediction, and channel estimation [8]–[10]. Furthermore, employing deep learning for performance prediction in IoT networks can expedite real-time configurations. DL-based models have the capability to precisely predict desired performance measurements from intricate datasets with high dimensionality, even in complex network scenarios and highly dynamic environments where mathematical derivations may not be practical.

A. Literature Survey

Recently, the studies of SPCs have been explored in non-orthogonal multiple access (NOMA) systems incorporating simultaneous transmitting and reflecting (STAR) reconfigurable intelligent surfaces (RIS) [11]. The average BLER, throughput, goodput, latency, reliability, and age of information of SPC-based unmanned aerial vehicle (UAV)-based NOMA systems were analyzed in [12], taking into account imperfect channel state information and successive interference cancellation. In order to achieve a good balance performance between cell-center users and cell-edge users while satisfying quality-of-service requirements, a hybrid long-and short-packet communication approach was investigated in [13]. In [14], the partial relay selection was proposed for dual-hop cooperative relaying networks with short packet communications. However, most of these recent works have just focused on half-duplex transmission in SPC environments. To improve the BLER and throughput of full-duplex IoT networks, the energy harvesting with hybrid power-time splitting protocol was designed for IoT devices with infinite and finite blocklength codes conditions [15]. A hybrid power-time splitting strategy with a non-linear energy harvesting model was also investigated in full-duplex cooperative IoT networks [16], where the reliability, goodput, and energy efficiency performances were analyzed. In [17], a performance analysis was conducted to compare

Manuscript received July 24, 2023; approved for publication January 18, 2024; approved for publication by Kim, Yun Hee Division 2 Editor, February 5, 2024.

T.-V. Nguyen is with the School of Computer Science and Engineering, International University, Ho Chi Minh City 700000, Vietnam, and also with Vietnam National University, Ho Chi Minh City, Vietnam, email: vannguyen-toan@gmail.com.

T. Huynh-The is with the Department of Computer and Communication Engineering, HCMC University of Technology and Education, Vietnam, email: thienht@hcmute.edu.vn.

V.-N. Q. Bao is with Posts and Telecommunications Institute of Technology, Ho Chi Minh 710372, Vietnam, email: baovnq@ptit.edu.vn.

V.-N. Q. Bao and T. Huynh-The are the corresponding authors.

A part of this paper has been accepted for presentation at the IEEE Statistical Signal Processing Workshop (SSP) 2023, Ha Noi, Vietnam, July 2-5, 2023 [1].

Digital Object Identifier: 10.23919/JCN.2024.000015

1229-2470/24/$10.00 © 2024 KICS

full-duplex relaying (FDR) and half-duplex relaying under SPC constraints. The finding results indicated that FDR was a favorable option for systems with lower transmit power, less strict block-error rate requirements, and effective mitigation of loop interference. However, different residual interference models have not yet been fully explored in these works.

The application of deep learning techniques to address complex optimization problems has been explored in the studies [8], [18]. Particularly, Hendra *et al.* in [18] proposed a deep learning approach to maximize spectral efficiency in multiple-input multiple-output (MIMO)-NOMA systems. On the other hand, Nguyen *et al.* [8] designed a new deep convolutional neural network (CNN) architecture to obtain the optimal solution for maximizing the achievable rate in multi-hop IoT systems. In [2], a DNN design for a relay selection scheme was shown to be more effective than the state-of-the-art machine learning models in predicting the throughput of cognitive IoT networks with a non-linear EH model. In [10], a novel CNN architecture was designed with feature enhancement-collection blocks to simultaneously predict the BLER and throughput of multi-hop SPC IoT systems with high accuracy and low execution time as compared to conventional CNN. In [19], the CNN was used for achieving solutions of downlink beamforming design of multiple-input single-output under the per-antenna power constraints. The practical testbed experiments of deep learning using software-defined radio were also built to demonstrate the effectiveness of the proposed system. However, these aforementioned works have not considered full-duplex transmission in conjunction with SPCs and deep learning designs in these IoT systems.

B. Motivation and Contributions

DL-based performance prediction in wireless energy transfer (WET) full-duplex IoT networks (WFINs) with different residual self-interference (RSI) models considering short-packet transmissions over Nakagami-*m* channels, which induces the intricacy of theoretical analysis, has not investigated in these previous works. This hinders a comprehensive investigation of the effects of RSI and finite block length under SPC studies. Moreover, when IoT networks are on a large-scale deployment, where the number of relays, and the number of antennas at the power beacon and destination are increasing exponentially with complex distributions. The traditional mathematical analysis of these systems may be intricate and these methods are not suitable for real-time applications in modern wireless communications systems. If we analyze the average BLER of the system with the RSI-II model, the resulting expression will have integral forms with several special functions (e.g., exponential integral function, gamma function, and Bessel functions), which cannot be further analyzed since they involved many complex functions. This motivates us to build a new framework relying on CNN design for performance evaluation. The DL framework allows us to estimate quickly the system performance, such as average BLER and throughput, whenever any changes in the network settings. The training process will be performed offline to obtain the trained model for online prediction, which helps to reduce the deployment time for network designing, planning, and monitoring in practice. We fill this gap by investigating full-duplex IoT networks consisting of multiple FD relays powered by a multi-antenna power beacon (PB) with different RSI models and evaluated by a new deep CNN architecture design. This work also emphasizes demonstrating the feasibility of a DL framework for efficiently evaluating WFINs wireless networks in which conventional mathematical model-based approaches become unfeasible. The main contributions of this paper can be summarized as follows:

- We propose a full relay selection (FRS) scheme in WFINs, where two RSI models are considered at the IoT devices under SPC constraints. We also derive new closed-form expressions for the average BLER and throughput of the FRS scheme over Nakagami-*m* fading channels with the RSI-I model under the considered system setup.
- We perform the approximation analysis of the average BLER and throughput of FRS scheme with the RSI-I model to show the effects of fading severity and locations of relay and power beacon on the system performance. The approximation approach has not been studied in recent works since the complexity of Nakagami-*m* fading channels.
- We develop a new deep convolutional neural network architecture to estimate the BLER and throughput of the FRS scheme with the RSI-II model, where a multi-output regression problem is designed to train network parameters for high-accuracy performance prediction.
- Simulation results reveal that the new CNN design provides the smallest root-mean-square error (RMSE) among the traditional designs such as the deep neural network (DNN) and conventional CNN approaches, emerging as an outstanding performance estimator in IoT networks.
- It is also revealed that the CNN-based scheme attains the same BLER and throughput as the FRS one, but with significantly reduced complexity. Additionally, the FRS scheme with RSI-I outperforms HD one in terms of BLER and throughput, which corroborates the efficiency of FD transmission.

The paper is organized as follows. Section II introduces the system model with two RSI scenarios and the relay selection strategy. The system performance analysis is provided in Section III focusing on average BLER and throughput. Section IV provides the new CNN design for BLER and throughput prediction of the FRS scheme. Section V provides simulations to confirm the theoretic results of Sections III and CNN design in IV. Section VI concludes the paper. The appendix provides proof of Lemma 1 with derivations of the theoretical results.

Mathematical Notations: Boldface represents vector and $\mathbb{E}\{\cdot\}$ are the expectation operator.

II. System Model

It is considered a wireless energy transfer full-duplex IoT system, where an IoT source (S) equipped with a single-antenna transmits short packets to a robot destination (D) with

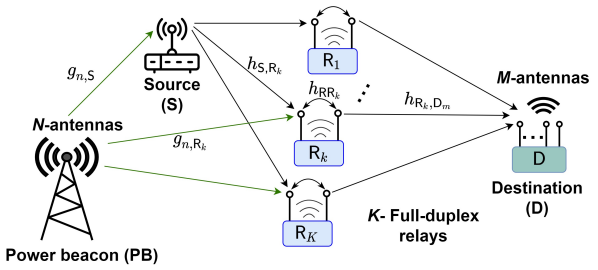

Fig. 1. A WET full-duplex IoT network.

M-antennas through SPC channels with the assistance of K FD relays $\mathcal{R} = \{\mathsf{R}_k\}_{k=1}^{K}$. At each relay, two isolated antennas are installed for transmission and reception, employing self-interference cancellation (SIC) to mitigate loop interference. However, RF impairments can prevent the complete elimination of residual self-interference [20], [21]. Being energy-constrained IoT devices, the source and relays use the harvested energy from an N-antenna power beacon to send their packets under the assumption of perfect CSI.

We denote by $g_{n,\mathsf{S}}$, g_{n,R_k}, with $n \in \{1, \cdots, N\}$, $h_{\mathsf{S},\mathsf{R}_k}$, and $h_{\mathsf{R}_k,\mathsf{D}_m}$, with $m \in \{1, \cdots, M\}$, the channel coefficients in the system from the n-antenna at power beacon to S and R_k, from S to R_k, and from R_k to D_m, respectively. Each channel coefficient is modeled as $f = \sqrt{G_f}\tilde{f}$ with $\tilde{f} \in \{g_{n,\mathsf{S}}, g_{n,\mathsf{R}_k}, h_{\mathsf{S},\mathsf{R}_k}, h_{\mathsf{R}_k,\mathsf{D}_m}\}$, where G_f represents the large-scale path loss and $\tilde{f}$ represents the small-scale fading following Nakagami-m fading model. Thus, the channel gain $|f|^2$ follows the gamma distribution with parameter λ_f. The large-scale path loss can be presented as $G_f = \sigma^{PL}(d/d_0)^{-\mathtt{PL}}$, where d, $\mathtt{PL}$, d_0, and σ^A are the distance between two nodes, the path loss exponent, the reference distance, and the power attenuation at d_0, respectively.

Different from long packet communications, which are usually based on the asymptotic Shannon theory, short packets with new coding rates require a different performance analysis approach. Short packets are subject to finite-blocklength effects, which means that the capacity rate and error probability depend on the blocklength and the channel conditions. In particular, the capacity rate expression using SPCs is a very complicated function of the transmission power and channel uses [8], making the design and evaluation of SPCs under the full-duplex scenarios with WET much more computationally challenging [22].

The system operation is divided into the WET and packet transmission (PT) phases. The period for the WET is $c_E T$ while that for PT is $(c_T - c_E)T$, where c_E, c_T, and T denote the number of channel uses (CUs) for the WET phase, the total number of CUs, and duration of each CU, respectively. In the WET phase, each IoT device will wirelessly harvest energy from the power beacon for the data transmission. We denote by $\eta \in (0, 1)$ and P, the energy conversion efficiency and the transmit power of each antenna at the PB, respectively. The energy harvested at each IoT device X, with $\mathsf{X} \in \{\mathsf{S}, \mathsf{R}_k\}$, from PB can be expressed as

$$E_{\mathsf{X}} = \eta c_E T P \sum_{n=1}^{N} |g_{n,\mathsf{X}}|^2, \tag{1}$$

where $g_{n,\mathsf{X}}$ is the channel coefficient between PB and X. After performing WET as in (1) during the period of $c_E T$, the transmit power of R_k over the PT period of $(c_T - c_E)T$ can be calculated as $P_{\mathsf{X}} = \frac{E_{\mathsf{X}}}{(c_T - c_E)T}$, which yields

$$P_{\mathsf{X}} = \frac{\eta c_E P}{c_T - c_E} \sum_{n=1}^{N} |g_{n,\mathsf{X}}|^2. \tag{2}$$

By using the FD transmission, the self-interference at R_k will include not only the additive white Gaussian noise, denoted by n_{R_k}, but also the RSI signal caused by the incomplete cancellation of the undesired interference, denoted by $u_{\mathtt{RSI}}$, which can be written as follows:

$$y_{\mathsf{RR}_k} = \sqrt{P_{\mathsf{S}}} h_{\mathsf{SR}_k} x_{\mathsf{S}} + u_{\mathtt{RSI}} x_{\mathsf{R}_k} + n_{\mathsf{R}_k}, \tag{3}$$

where $u_{\mathtt{RSI}}$ is the RSI signal at R_k, x_{S} and x_{R_k} denote the signals at the S and R_k, respectively.

The RSI in (3) can affect the quality and reliability of the desired signal and thus needs to be modeled and mitigated properly. Therefore, we consider $u_{\mathtt{RSI}}$ with two models such as RSI-I and RSI-II as follows:

- (I) RSI-I model: $u_{\mathtt{RSI}}$ in (3) is zero-mean, additive and Gaussian following $\mathcal{CN}(0, l\sigma_k^2)$, where l reflects the quality of the SIC technique and σ_k^2 is the RSI variance [20], [23]. The smaller value of l indicates a better self-interference cancellation quality. The RSI-I model has zero-mean, which implies that there is no bias or offset in the RSI model since its average value is zero. It is Gaussian means that the RSI-I model has a normal distribution with zero-mean and variance of $l\sigma_k^2$. If the interference is not Gaussian, the RSI-I model can be seen as the worst-case scenario in terms of achievable rate [24]. The Gaussian assumption might hold in reality due to the various sources of imperfections in the cancellation process (i.e., due to the central limit theorem). Moreover, it is additive indicating that it is added to the desired signal as the external noise at the receiver. This implies that the RSI can be treated as an independent noise source and its effect can be analyzed using standard techniques such as signal-to-interference-plus-noise ratio (SINR) or error probability [25].
- (II) RSI-II model: $u_{\mathtt{RSI}}$ is an independent Nakagami-m random variable and can be presented as $u_{\mathtt{RSI}} = \sqrt{P_{\mathsf{R}}} h_{\mathsf{RR}_k}$, where h_{RR_k} is the SI channel at R_k. Thus, $|h_{\mathsf{RR}_k}|^2$ follows gamma distribution with spread parameter λ_R and shape parameter m_3. The shape parameter influences the shape of the distribution, while the spread parameter controls the scale of the distribution. Modeling RSI as a Nakagami-m fading channel can capture various fading scenarios, but it also introduces high mathematical complexity due to the involvement of Gamma functions and incomplete

Gamma functions. Therefore, several existing works used approximations or bounds to simplify the analysis, but these approaches may lose accuracy [26].

From (3), the instantaneous SNR at relays is expressed as

$$\gamma_{\mathsf{SR}_k} = \frac{\kappa\psi \sum_{n=1}^{N} |g_{n,\mathsf{S}}|^2 |h_{\mathsf{S},\mathsf{R}_k}|^2}{z_{\mathtt{RSI}} + 1}, \tag{4}$$

where $\kappa \triangleq \eta c_E/(c_T - c_E)$, $\psi = P/\sigma_n^2$, $z_{\mathtt{RSI}} = \sigma_k^2/\sigma_n^2$ for RSI-I model, and $z_{\mathtt{RSI}} = P_{\mathsf{R}}|h_{\mathsf{RR}_k}|^2/\sigma_n^2$ for RSI-II model. The maximal ratio combining is used at the robot destination, and the instantaneous SNR at D_m can be expressed as

$$\gamma_{\mathsf{R}_k\mathsf{D}_m} = \kappa\psi \sum_{n=1}^{N} |g_{n,\mathsf{R}_k}|^2 \sum_{m=1}^{M} |h_{\mathsf{R}_k,\mathsf{D}_m}|^2. \tag{5}$$

By using the decode-and-forward protocol, an FD relay is chosen to achieve the highest end-to-end (e2e) SNR, i.e.,

$$\mathsf{R}_{k^*} = \arg \max_{k=1,\cdots,K} \min\{\gamma_{\mathsf{SR}_k}, \gamma_{\mathsf{R}_k\mathsf{D}_m}\}. \tag{6}$$

The criterion (6) will improve reliable packet communication in WFINs under short blocklength transmission and imperfection of the SI channels. The e2e SNR of the considered network can be expressed as

$$\gamma_{e2e} = \max_{k=1,\cdots,K} \min\{\gamma_{\mathsf{SR}_k}, \gamma_{\mathsf{R}_k\mathsf{D}_m}\}. \tag{7}$$

Based on the e2e SNR, the average BLER, throughput, reliability, and latency will be analyzed in the following section.

III. Performance Analysis

1) BLER Analysis: Assuming finite blocklength transmission through channel $i \in \{\mathsf{SR}_k, \mathsf{R}_k\mathsf{D}_m\}$, the S transmits τ information bits (message size) encoded into a packet over the blocklength $t > 100$. The received SNR and the channel coding rate are denoted as γ_i and $r_i \triangleq \tau/t$, respectively, the average BLER can be calculated as

$$\varepsilon_i \approx \int_0^\infty \left[Q\left(\frac{C(\gamma_i) - r_i}{\sqrt{V(\gamma_i)/t}}\right)\right] f_{\gamma_i}(x)dx, \tag{8}$$

where $Q^{-1}(.)$ denotes the inverse Gaussian Q-function, $V(x) \triangleq (1 - (1+x)^{-2})(\log_2 e)^2$ is the channel dispersion, and $C(x) \triangleq \log_2(1+x)$ is the Shannon capacity. The involvement of a complex Gaussian Q-function in (8) makes the exact closed-form expression for the system BLER quite complex. A tight approximation method for Q-function will be used to solve integral in (8), where the Q-function is approximated as $Q\left(\frac{C(\gamma_i)-r_i}{\sqrt{V(\gamma_i)/t}}\right) \approx \Xi(\gamma_i)$, with $\Xi(\gamma_i)$ being expressed as [8], [16], [17]

$$\Xi(\gamma_i) = \begin{cases} 1, & \gamma_i \le v_i, \\ 0.5 - \delta_i\sqrt{t}(\gamma_i - \zeta_i), & v_i \le \gamma_i \le u_i, \\ 0, & \gamma_i \ge u_i, \end{cases} \tag{9}$$

where $\delta_i = [2\pi(2^{2r_i} - 1)]^{-1/2}$, $v_i = \zeta_i - 1/(2\delta_i\sqrt{t})$, $\zeta_i \triangleq 2^{r_i} - 1$, and $u_i = \zeta_i + 1/(2\delta_i\sqrt{t})$. Using this feasible approximation, ε_i can be calculated as

$$\varepsilon_i = \int_0^\infty \Xi(\gamma_i) f_{\gamma_i}(x)dx \overset{(a)}{=} \delta_i\sqrt{t} \int_{v_i}^{u_i} F_{\gamma_i}(x)dx, \tag{10}$$

where $F_{\gamma_i}(.)$ is the cumulative distribution function (CDF) of γ_i and step (a) is due to the integration by parts. Making use of the first order Riemann integral approximation, i.e., $\int_x^y f(z)dz = (y-x)f(\frac{x+y}{2})$, for (10), which yields

$$\varepsilon_i(\zeta_i) = F_{\gamma_i}(\zeta_i). \tag{11}$$

Next, we find the CDF of γ_i of the considered FD system based on the criterion (6).

Theorem 1. *The CDFs of γ_{SR_k} and $\gamma_{\mathsf{R}_k\mathsf{D}_m}$ over Nakagami-m fading channels with RSI-I model are expressed, respectively, as*

$$F_{\gamma_{\mathsf{SR}_k}}(x) = 1 - \sum_{t=0}^{m_1 N-1} \frac{2}{t!\Gamma(m_2)} \left(\frac{m_1\lambda_{E,1}m_2\lambda_{D,1}x}{(z_{\mathtt{RSI}}+1)^{-1}\kappa\psi}\right)^{\frac{m_2M+t}{2}} \times K_{m_2-t}\left(2\sqrt{\frac{m_1\lambda_{E,1}m_2\lambda_{D,1}x}{(z_{\mathtt{RSI}}+1)^{-1}\kappa\psi}}\right), \tag{12}$$

$$F_{\gamma_{\mathsf{R}_k\mathsf{D}_m}}(x) = 1 - \sum_{t=0}^{m_1 N-1} \frac{2}{t!\Gamma(m_2M)} \left(\frac{m_1\lambda_{E,2}m_2\lambda_{D,2}x}{\kappa\psi}\right)^{\frac{m_2M+t}{2}} \times K_{m_2M-t}\left(2\sqrt{\frac{m_1\lambda_{E,2}m_2\lambda_{D,2}x}{\kappa\psi}}\right). \tag{13}$$

Proof: Please see Appendix A. ∎

From (11), (12), and (13), the e2e BLER of the considered system can be expressed as

$$\varepsilon_{e2e} = \prod_{k=1}^{K} [\varepsilon_{\mathsf{SR}_k}(\zeta_{\mathsf{SR}_k}) + \varepsilon_{\mathsf{R}_k\mathsf{D}_m}(\zeta_{\mathsf{R}_k\mathsf{D}_m}) - \varepsilon_{\mathsf{SR}_k}(\zeta_{\mathsf{SR}_k})\varepsilon_{\mathsf{R}_k\mathsf{D}_m}(\zeta_{\mathsf{R}_k\mathsf{D}_m})]. \tag{14}$$

Based on Theorem 1, when the fading severity parameters of EH links and the number of antennas at the PB increase, their product inside the Bessel function is large, making the CDFs of γ_{SR_k} and $\gamma_{\mathsf{R}_k\mathsf{D}_m}$ become small. However, these expressions are still in the Bessel function, and difficult to draw some insights into the system behavior directly. Therefore, we will perform the approximation analysis for the average BLER in the following Theorem.

Theorem 2. *The approximated CDFs of γ_{SR_k} and $\gamma_{\mathsf{R}_k\mathsf{D}_m}$ over Nakagami-m fading channels with RSI-I model are expressed, respectively, as*

$$F^{\mathtt{ap}}_{\gamma_{\mathsf{SR}_k}}(x) = 1 - \sum_{t=0}^{m_1 N-1} \sum_{n=0}^{I} \sum_{i=0}^{n} \frac{\exp(-2\sqrt{\Delta_1 x})}{t!\Gamma(m_2)} \times \Upsilon(\Delta_1 x, m_2, t, n, i), \tag{15}$$

$$F^{\mathtt{ap}}_{\gamma_{\mathsf{R}_k\mathsf{D}_m}}(x) = 1 - \sum_{t=0}^{m_1 N-1} \sum_{n=0}^{I} \sum_{i=0}^{n} \frac{\exp(-2\sqrt{\Delta_2 x})}{t!\Gamma(m_2M)} \times \Upsilon(\Delta_2 x, m_2M, t, n, i), \tag{16}$$

where

$$\Delta_1 = \frac{m_1\lambda_{E,1}m_2\lambda_{D,1}}{(z_{\mathsf{RSI}}+1)^{-1}\kappa\psi}, \quad \Delta_2 = \frac{m_1\lambda_{E,2}m_2\lambda_{D,2}}{\kappa\psi}, \tag{17}$$

$$\Upsilon(a,b,c,n,i) = \begin{cases} 2^{1+i-|b-c|}(\sqrt{a})^{i+2\min(b,c)}\Lambda(|b-c|,n,i), \\ \qquad when \quad b-c \neq 0, \\ 2^{i-1}(\sqrt{a})^{b+c+i-2}[\Lambda(2,n,i) - 2\Lambda(1,n,i)], \\ \qquad when \quad b-c = 0, \end{cases} \tag{18}$$

$$\Lambda(Q,n,i) = \frac{(-1)^i\sqrt{\pi}\Gamma(2Q)\Gamma(0.5+n-Q)L(n,i)}{2^{M-i}\Gamma(0.5-Q)\Gamma(0.5+n+Q)n!}, \tag{19}$$

$$L(n,i) = \binom{n-1}{i-1}\frac{n!}{i!}, L(0,0) = 1, L(n,0) = 0, L(n,1) = n!. \tag{20}$$

Proof: Please see Appendix B. ∎

In Theorem 2, the CDFs of γ_{SR_k} and $\gamma_{\mathsf{R}_k\mathsf{D}_m}$ are shown as exponential functions of fading severity parameters m_1, m_2, and the channel uses for EH through parameters Δ_1 and Δ_2. The number of antennas at D and PB is proportional to the CDFs of γ_{SR_k} and $\gamma_{\mathsf{R}_k\mathsf{D}_m}$. The positions of PB and FD relays expressed through parameters $\lambda_{E,1}$ and $\lambda_{E,2}$ also considerably influence the CDFs of γ_{SR_k} and $\gamma_{\mathsf{R}_k\mathsf{D}_m}$, which will be extensively evaluated in the numerical results Section. Similar to (11), the approximation of BLER is expressed as

$$\varepsilon_i^{\mathsf{ap}}(\zeta_i) = F_{\gamma_i}^{\mathsf{ap}}(\zeta_i). \tag{21}$$

The e2e BLER approximation of the considered system can be expressed as

$$\varepsilon_{e2e}^{\mathsf{ap}} \approx \prod_{k=1}^{K}[\varepsilon_{\mathsf{SR}_k}^{\mathsf{ap}}(\zeta_{\mathsf{SR}_k}) + \varepsilon_{\mathsf{R}_k\mathsf{D}_m}^{\mathsf{ap}}(\zeta_{\mathsf{R}_k\mathsf{D}_m})]. \tag{22}$$

Compared to the e2e BLER in (14), the product of two error probabilities, $\varepsilon_{\mathsf{SR}_k}^{\mathsf{ap}}(\zeta_{\mathsf{SR}_k})$ and $\varepsilon_{\mathsf{R}_k\mathsf{D}_m}^{\mathsf{ap}}(\zeta_{\mathsf{R}_k\mathsf{D}_m})$, is very small, approximating $10^{-4}-10^{-6}$, when $\psi \to \infty$ in (22); thus, this product can be ignored.

2) Throughput Analysis: The system throughput R_{th} can be formulated by considering the delay-limited transmission with a fixed data transmission rate in bits per channel use (BPCU) as

$$\tau_{e2e} = R_{th}(1-\varepsilon)(c_T - c_E)/c_T, \tag{23}$$

where $\varepsilon \in \{\varepsilon_{e2e}, \varepsilon_{e2e}^{\mathsf{ap}}\}$, and $(c_T - c_E)/c_T$ presents the fraction of effective communication time and total transmission time.

Regarding the RSI-II model, the analysis of average BLER is quite intricate since it involves four random variables leading to the integral of the product of two Bessel functions. This challenge motivates us to build a new framework relying on deep learning design for performance evaluation. The new DL framework is projected to estimate the average BLER and throughput of the FRS scheme with the RSI-II model via a short-time inference process, which contributes to reducing the deployment time for network designing, planning, and monitoring in practice. The proposed DL framework will be presented in the next section.

TABLE I
TRAINING INPUT VARIABLES AND RESPECTIVE VALUES FOR CNN.

Variable	Value	Variable	Value
K	$[2,6]$	y_{PB}	$[2,6]$
N	$[2,5]$	P_{PB}	$[5,30]$
M	$[2,6]$	c_E	$[350,400]$
x_{R}	$[8,13]$	R_{th}	$[0.5,1.5]$
y_{R}	$[0,4]$	τ	$[500,600]$
x_{PB}	$[8,12]$		

IV. PROPOSED CNN DESIGN FOR BLER AND THROUGHPUT PREDICTION

We propose a deep CNN design to predict the average BLER and throughput of the considered system with the RSI-II scenario. The proposed CNN includes an input layer with a size of 1×11 for processing network parameters. The input variables consist of the number of relays (K), the number of antennas at PB (N), the number of antennas at D (M), the positions of relay (x_{R} and y_{R}), the position of PB (x_{PB} and y_{PB}), the transmit power of PB (P_{PB}), the channel uses for EH (c_E), the information bits τ, and the target data rate (R_{th}). We have chosen the above system parameters because they influence significantly the performance of the proposed WFINs. Over $160,000$ samples are generated for training and testing based on input variables in Table I.

An input sample to the deep network for BLER and throughput estimation can be expressed as follows:

$$\mathbf{x} \triangleq [K, N, M, x_{\mathsf{R}}, y_{\mathsf{R}}, x_{\mathsf{PB}}, y_{\mathsf{PB}}, P_{\mathsf{PB}}, c_E, \tau, R_{th}]. \tag{24}$$

The proposed CNN architecture is illustrated in Fig. 2, where the input size is specified as 1×11, representing the wireless system variables outlined in Table I. Following this, a convolutional (conv) layer with a kernel size of 1×1 is employed, succeeded by a batch normalization (bn) layer and a swish activation (swish) layer to aggregate features across three color channels. To capture more diversified features, we design an MRF block with three parallel connections, each of which is specified by a conv layer with the kernel size of 1×1, followed by a conv layer with different one-dimensional asymmetric kernels of sizes such as 1×3, 1×2, and 1×1. The bn and swish layers are used in each connection, where their outputs are subsequently collected along the depth dimension using a depth-wise concatenation (concat) layer to merge the outputs. To reduce computational expenses when the network goes deeper, a max-pooling layer (maxpool) with a stride of $(1,2)$ and a pool size of 1×2 is employed. This operation effectively reduces the spatial dimensions of the feature maps by half [27].

In order to highlight the significant features obtained from the previous layers, multiple processing $\mathrm{P}-\mathrm{Blocks}$ are linked together in a serial manner to extract intrinsic features as the correlations between system variables, which are interleaved by a (maxpool) layer to decrease the dimension of feature maps. Each $\mathrm{P}-\mathrm{Block}$ has three conv layers and an element-wise addition add layer. These layers are connected by following the structure of residual blocks of ResNet [28], which has been broadly applied to address the vanishing gradient

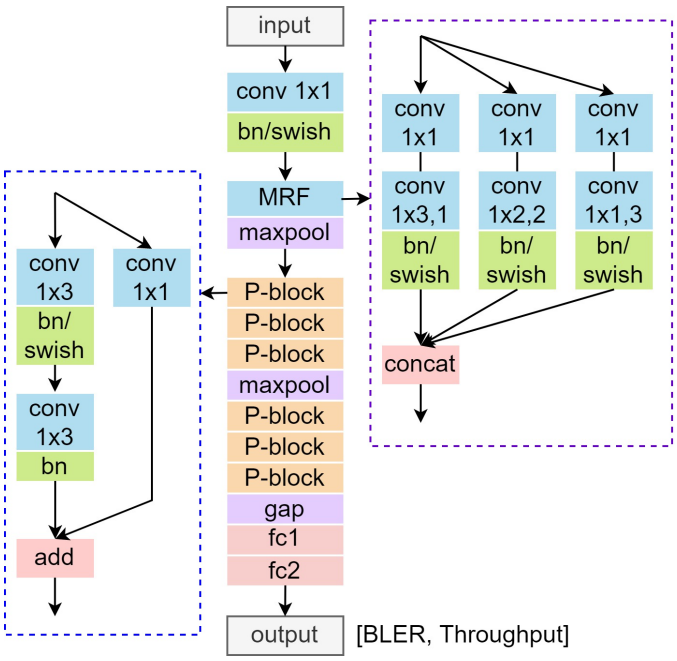

Fig. 2. The proposed CNN architecture for BLER and throughput prediction.

problem in numerous learning tasks of wireless communications [29]. To further collect meaningful features, the outputs are then traveled to the next three $\mathrm{P}-\mathrm{Blocks}$, ended with a global average pooling (gap) layer, and followed by two fully connected (fc) layers to summarize spatial features in each map and estimate continuous values of BLER and throughput. The loss function of the regression problem measures the discrepancy between the predicted value, denoted by $\mathbf{y}_{(t)}$, and true target value, denoted by $\tilde{\mathbf{y}}_{(t)}$, what can be presented as [9]

$$\mathrm{Loss} = \frac{1}{S_t}\sum_{t=1}^{S_t}(\mathbf{y}_{(t)} - \tilde{\mathbf{y}}_{(t)})^2, \tag{25}$$

where S_t is the number of samples for training. The weights and biases of the CNN have been updated during the back-propagation process using the Adam optimizer.

Once the offline training process is finished, the resulting CNN model, comprising weights and biases, can be succinctly represented as a concise mapping function denoted as $\mathcal{F}(.)$. Typically, a well-trained CNN is capable of providing highly precise and real-time predictions. Thus, the obtained CNN model is used to predict the BLER and throughput values when any new data becomes available at the input. Particularly, each input sample, sorted into vector $\mathbf{x}$, at the input of CNN, the CNN will produce the respective output values of BLER and throughput, also arranged into vector $\tilde{\mathbf{y}} \triangleq [\tilde{\varepsilon}_{e2e}\ \tilde{\tau}_{e2e}]$, i.e.,

$$\tilde{\mathbf{y}} = \mathcal{F}(\mathbf{x}). \tag{26}$$

Through this short-time inference procedure, the CNN model can predict both the BLER and throughput within a short time.

V. Numerical Results and CNN Evaluation

In this section, we provide some illustrative examples for system performance evaluation. Monte Carlo simulations and CNN prediction results of the BLER and throughput are presented to verify our designed approach. The S, D, R_k, and PB are located, respectively, at $(0,0)$, $(15,0)$, $(10,0)$, and $(10,3)$ on the Euclidean plane. We set $d_0 = 1$ m, $\sigma^{PL} = -30$ dB, the shape parameters $m_1 = m_2 = m_3 = 2$, $\mathtt{PL} = 3.6$. Unless otherwise specified, the remaining simulation parameters are set as follows. $K = 3$, $M = 3$, $N = 3$, $c_T = 900$, the number of bits 600, $c_E = 400$, $\eta = 0.8$, $l = 0.01$, $I = 12$, and the normalized noise variance $\sigma^2 = 1$. The whole dataset is divided by 80% and 20% for training and testing, respectively. The CNN is trained for 60 epochs with random weights initialization, a gradient decay factor of 0.96, and the adaptive moment estimation optimizer. At the beginning of the training phase, the learning rate is initial with 10^{-3} and it is decreased by 90 % after 20 epochs.

For the multiple output regression, the RMSE is used for the performance evaluation of the CNN design in predicting the BLER and throughput. RMSE measures the deviation between the true target and predicted values across the whole test set. By considering the samples in the test set, the RMSE can be calculated as

$$\mathrm{RMSE} = \sqrt{\mathbb{E}\{(\mathbf{y} - \tilde{\mathbf{y}})^2\}}. \tag{27}$$

Fig. 3 illustrates the effects of the percentage of training data on different deep models. The first model is a DNN with five fully-connected layers, each of which consists of 256 neurons. The second model is a traditional CNN with a straightforward architecture involving six conv layers (utilizing 1×3 with the numbers of filters of 64, 64, 128, 128, 256, and 256), followed by activation ReLU layers and interleaved by max-pooling layers. As can be observed, the proposed CNN achieves the lowest RMSE while the deep neural network gets the highest RMSE when the percentage of training data increases. The reason is that the DNN model with a simple structure is not able to estimate a moderate-to-high-dimensional dataset, leading to the lowest performance. Although the traditional CNN performs BLER and throughput prediction more accurately than DNN, it is limited by multiple input correlations and vanishing gradients if compared with the proposed CNN model. Furthermore, it is realized that the RMSE of the CNN models decreases more significantly than that of the DNN ones as the amount of training data increases. DNNs are usually more prone to overfitting than CNNs, especially when dealing with large amounts of data, because DNNs have more parameters, thus leading to the model memorizing the training data rather than learning generalizable patterns. Besides the ability to capture local patterns, reduced dimensionality, and parameter efficiency, the proposed CNN model can map the original dataset into a higher dimensional space with complex patterns, resulting in error reduction and estimation accuracy improvement. Due to the lowest RMSE of the proposed CNN, it will be used for predicting the average BLER and throughput in the next simulations.

As shown in Fig. 4, the FD scheme with the RSI-I model delivers the best performance compared to the half-duplex

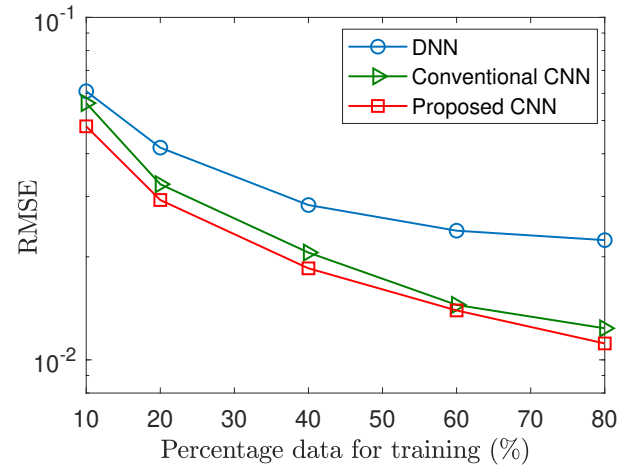

Fig. 3. Effects of the percentage of data samples for training on the RMSE.

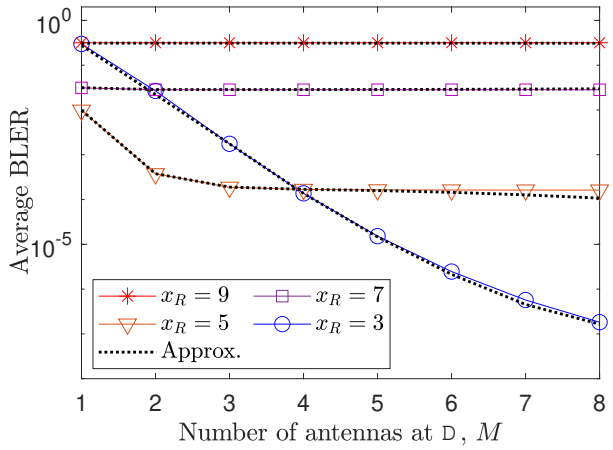

Fig. 5. Effects of M on the average BLER of RSI-I model-based FRS scheme with the position of PB being $(11, 5)$ and $N = 2$.

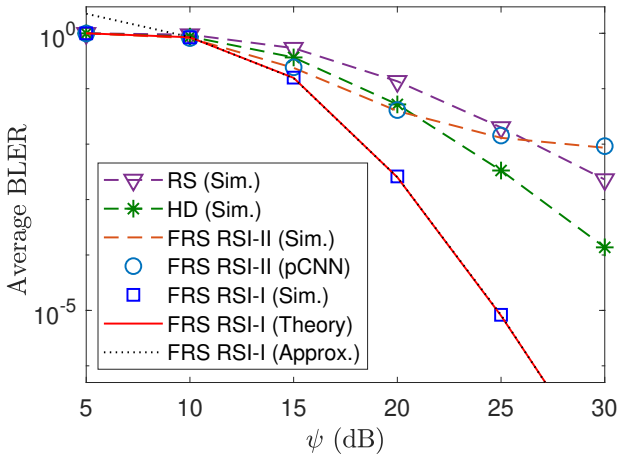

Fig. 4. Average BLER of different schemes.

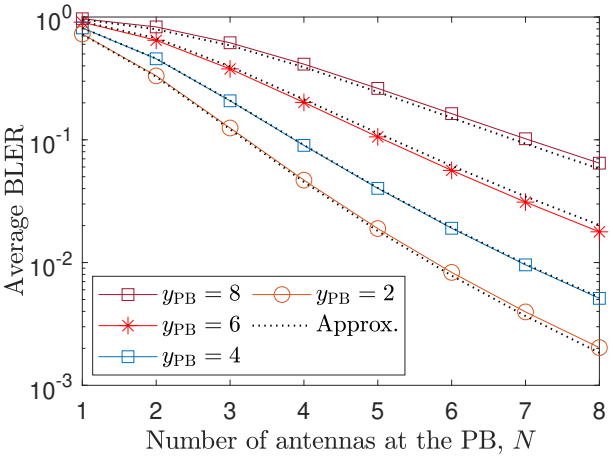

Fig. 6. Effects of N on the average BLER of RSI-I model-based FRS scheme with $\psi = 15$ dB.

scheme, highlighting the benefits of full-duplex transmission. Furthermore, the FRS scheme, which involves multiple relays in the relay selection process, achieves higher diversity and reliable transmissions than the random relay selection (RS) scheme, resulting in lower BLER. Furthermore, the Monte-Carlo simulations of the FRS scheme with the RSI-I model demonstrate excellent agreement with the analytical ones, affirming the correctness of the developed analysis. The approximation results are also tightly matched to the analysis one, validating our approximation approach. Moreover, the CNN prediction results of the RSI-II model closely align with the simulation ones, emphasizing the efficacy of CNN design in Section IV.

Fig. 5 reveals the effects of the number of antennas at D on the system BLER with different positions of FD relays. As can be observed, the number of antennas at D significantly affects the average BLER when the relay is closer to the source, but it does not affect the system BLER when the relay is farther from the source. The reason is that the e2e SNR is dominated by the instantaneous SNR at the relay, γ_{SR_k}, in (6) when the distance between S and R_k is large, and increasing M does not improve the e2e SNR. On the other hand, when the distance from source to relay is small, leads to the domination of instantaneous SNR at D, $\gamma_{\mathsf{R}_k\mathsf{D}_m}$, in (6), and the e2e SNR is now a function of M.

Fig. 6 shows the significant effect of the number of antennas at the PB on the average BLER of FRS scheme with the RSI-I model. When the position of PB is close to the network, or when a greater number of antennas are deployed at the PB, the source and FD relays have more opportunities to harvest energy, which improves the average BLER. Moreover, when N is large, more degrees of freedom are contributed to the system. Thus, the improvement of the average BLER becomes significant when the PB is located near the network.

Fig. 7 shows the increase of throughput of all schemes as ψ is large. The S and R_k will have more chances of harvesting sufficient energy from the PB when ψ is large, which results in the improvement of throughput. Again, the FRS scheme with the RSI-I model achieves the highest throughput, while the HD scheme yields the lowest performance. Furthermore, the CNN-based scheme achieves the same throughput as the FD

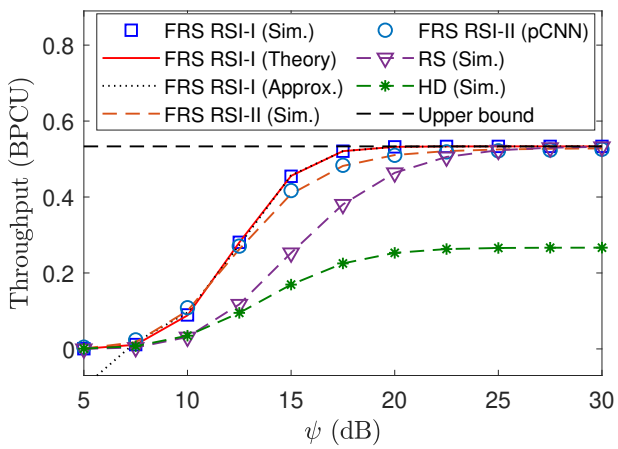

Fig. 7. Throughput of different schemes.

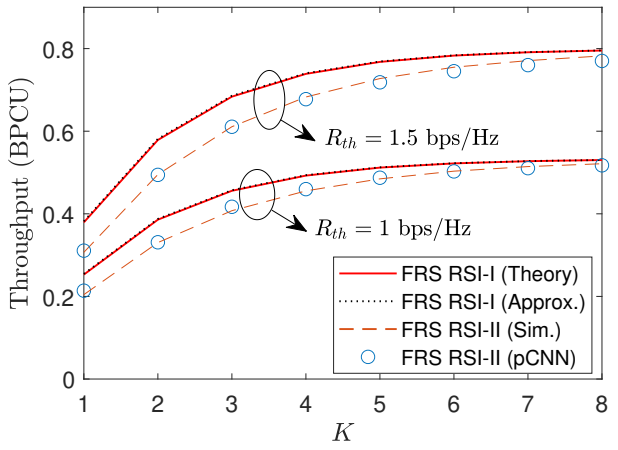

Fig. 8. Effect of K on the throughput of different schemes.

RSI-II model, showing an exceptional CNN design approach.

Fig. 8 shows the effects of the number of FD relays and R_{th} on the throughput of FRS scheme. When R_{th} is increased, the average throughput of FRS scheme with RSI-I and RSI-II models considerably improves. When K is large, the system with the RSI-I model achieves almost the same throughput as its counterpart with the RSI-II one. It also shows that the CNN prediction of the RSI-II model is matched with the simulation one. This shows the correctness of our CNN design framework.

The reliability and latency of short-packet communications [6], [8], [10] can be calculated as

$$\text{Reliability} = (1 - \varepsilon_{e2e}) \times 100\%, \tag{28}$$

$$\text{Latency} = (c_T - c_E)T/(1 - \varepsilon_{e2e}), \tag{29}$$

where $T = 3\mu s$ [30].

In Fig. 9, it can be observed that the message containing 256 bytes demonstrates greater reliability and lower latency compared to longer messages (i.e., those consisting of 512 or 1024 bytes). The message with the size of 512 byte can be encoded into packets over 6000 CUs to increase the

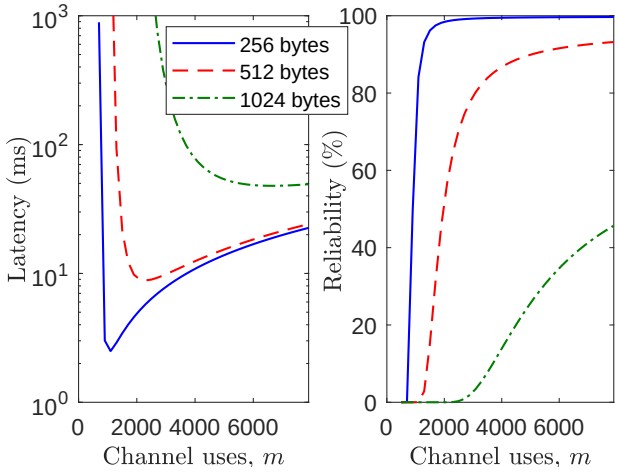

Fig. 9. The reliability and latency of FRS scheme with RSI-I.

TABLE II
COMPARISON OF EXECUTION TIME FOR THE BLER AND THROUGHPUT EVALUATION OF FRS SCHEME WITH RSI-II SCENARIO BETWEEN SIMULATION USING MONTE-CARLO (SIM-MC) AND PREDICTION USING CNN (PREDICT-CNN) DESIGN, WITH $\psi = 20$ dB.

Scenarios $\{K, N, M, c_E\}$	Sim-MC	Predict-CNN	RMSE
$\{3, 2, 3, 350\}$	4.8132 s	0.003828 s	0.0012
$\{5, 4, 5, 370\}$	12.835 s	0.004978 s	0.0020
$\{7, 6, 7, 400\}$	24.754 s	0.005375 s	0.0054

reliability level to 90%, as shown in Fig. 9(b). However, its latency amounts to approximately 20 seconds, as indicated in Fig. 9(a), which surpasses the maximum allowed latency for URLLC services and applications [4]. On the other hand, the 1024-byte message exhibits a latency of 80 seconds and a reliability of less than 40% with the utilization of 6000 channel uses, failing to meet the stringent requirements for both latency and reliability. Consequently, it can be concluded that longer messages are unsuitable for supporting URLLCs in IoT networks and for facilitating low-delay communications in factory automation.

Finally, the running time of the throughput prediction is evaluated in Table II. To obtain the exact result at $\psi = 20$ dB, each sample of Monte-Carlo is averaged over 3×10^6 trials. In all scenarios, when parameters K, N, M, and c_E of the considered system increase, the CNN consistently predicts the BLER and throughput with a short period of time less than 6ms. In contrast, the running time of the simulation method grows rapidly with such parameters, taking over 24 s for the last case. Numerical results show the outstanding capability of the CNN-based scheme to effectively handle IoT networks with large-scale configurations.

VI. CONCLUSIONS

We studied the performance analysis of FEINs, where different RSI models for full-duplex IoT devices were considered. The full relay selection was proposed to achieve the highest e2e SNR of the system with the RSI-I model, based on which the closed-form expression for the average BLER

and throughput were derived. The respective approximation analysis was also carried out to provide deeper insights into the system behavior. Aimed real-time configurations, a CNN architecture was designed for estimating the average BLER and throughput when mathematical analyses of the system with the RSI-II model became intricate. Simulation results demonstrated that the CNN design-based estimation scheme attained the exact average BLER and throughput values of the FRS RSI-II model. Our future works will investigate the FD-enabled multi-hop SPC incorporating new network paradigms such as reflecting surface and edge computing to enable distributed learning for future IoT systems.

APPENDIX A
PROOF OF THEOREM 1

We first consider (4) with RSI-I model, i.e., $z_{\mathtt{RSI}} = \sigma_k^2/\sigma_n^2$, let $X = \sum_{n=1}^{N} |g_{n,\mathsf{S}}|^2$, the CDF of γ_{SR_k} can be calculated as

$$F_{\gamma_{\mathsf{SR}_k}}(x) = \Pr\left[\frac{\kappa\psi X|h_{\mathsf{S},\mathsf{R}_k}|^2}{z_{\mathtt{RSI}}+1} < x\right] = \int_0^{\infty} F_X\left(\frac{x(z_{\mathtt{RSI}}+1)}{\kappa\psi w}\right) f_{|h_{\mathsf{S},\mathsf{R}_k}|^2}(w)dw, \quad (30)$$

where $F_X(.)$ and $f_{|h_{\mathsf{S},\mathsf{R}_k}|^2}(.)$ denote the CDF of X and PDF of $|h_{\mathsf{S},\mathsf{R}_k}|^2$, respectively. Over Nakagami-m fading channels, $F_X(.)$ and $f_{|h_{\mathsf{S},\mathsf{R}_k}|^2}(.)$ can be expressed, respectively, as

$$F_X(x) = 1-\exp(-m_1\lambda_{E,1}x)\sum_{t=0}^{m_1N-1}\frac{(m_1\lambda_{E,1}x)^t}{t!}, \quad (31)$$

$$f_{|h_{\mathsf{S},\mathsf{R}_k}|^2}(x) = \frac{(m_2\lambda_{D,1})^{m_2}x^{m_2-1}}{\Gamma(m_2)}\exp(-m_2\lambda_{D,1}x). \quad (32)$$

Plugging (31) and (32) into (30) and after some manipulations, we obtain as

$$F_{\gamma_{\mathsf{SR}_k}}(x) \quad (33)$$

$$= 1-\sum_{t=0}^{m_1N-1}\frac{(m_2\lambda_{D,1})^{m_2}}{t!\Gamma(m_2)}\left(\frac{m_1\lambda_{E,1}x}{(z_{\mathtt{RSI}}+1)^{-1}\kappa\psi}\right)^t \quad (34)$$

$$\times\int_0^{\infty} w^{m_2-t-1}\exp\left(-\frac{m_1\lambda_{E,1}x}{(z_{\mathtt{RSI}}+1)^{-1}\kappa\psi w} - m_2\lambda_{D,1}w\right)dw.$$

By applying [31, Eq. (3.471.9)], the integral of (33), denoted by T_1, can be calculated as

$$T_1 = 2\left(\frac{m_1\lambda_{E,1}x(z_{\mathtt{RSI}}+1)}{\kappa\psi m_2\lambda_{D,1}}\right)^{\frac{m_2-t}{2}} \quad (35)$$

$$\times K_{m_2-t}\left(2\sqrt{\frac{m_1\lambda_{E,1}m_2\lambda_{D,1}x}{\kappa\psi(z_{\mathtt{RSI}}+1)^{-1}}}\right). \quad (36)$$

By substituting (35) into (33) and after some manipulations, we obtain the CDF of γ_{SR_k} as shown in (12).

Next, we consider (5), let $Y = \sum_{m=1}^{M}|h_{\mathsf{R}_k,\mathsf{D}_m}|^2$ and $Z = \sum_{n=1}^{N}|g_{n,\mathsf{R}_k}|^2$, the CDF of $\gamma_{\mathsf{R}_k\mathsf{D}_m}$ can be calculated as

$$F_{\gamma_{\mathsf{R}_k\mathsf{D}_m}}(x) = \Pr[\kappa\psi YZ < x] = \int_0^{\infty} F_Z\left(\frac{x}{\kappa\psi y}\right) f_Y(y)dy. \quad (37)$$

The CDF of Z and PDF of Y in (37) can be expressed, respectively, as

$$F_Z(x) = 1-\exp(-m_1\lambda_{E,2}x)\sum_{t=0}^{m_1N-1}\frac{(m_1\lambda_{E,2}x)^t}{t!}, \quad (38)$$

$$f_Y(x) = \frac{(m_2\lambda_{D,2})^{m_2M}x^{m_2M-1}}{\Gamma(m_2M)}\exp(-m_2\lambda_{D,2}x). \quad (39)$$

Next, by plugging (38) and (39) into (37), we obtain as

$$F_{\gamma_{\mathsf{R}_k\mathsf{D}_m}}(x) \quad (40)$$

$$= 1-\sum_{t=0}^{m_1N-1}\frac{(m_2\lambda_{D,2})^{m_2M}}{t!\Gamma(m_2M)}\left(\frac{m_1\lambda_{E,2}x}{\kappa\psi}\right)^t \quad (41)$$

$$\times\int_0^{\infty} y^{m_2M-t-1}\exp\left(-\frac{m_1\lambda_{E,2}x}{\kappa\psi y} - m_2\lambda_{D,2}y\right)dy.$$

Similar to steps to calculate (33), the integral in (40), denoted by T_2, can be calculated by applying [31, Eq. (3.471.9)] as follows:

$$T_2 = 2\left(\frac{m_1\lambda_{E,2}x}{\kappa\psi m_2\lambda_{D,2}}\right)^{\frac{m_2M-t}{2}}K_{m_2M-t}\left(2\sqrt{\frac{m_1\lambda_{E,2}m_2\lambda_{D,2}x}{\kappa\psi}}\right). \quad (42)$$

Plugging (42) into (40), and after some manipulations, the CDF of $\gamma_{\mathsf{R}_k\mathsf{D}_m}$ can be obtained as (13). The proof is complete.

APPENDIX B
PROOF OF THEOREM 2

By applying Lemma 1 in [8], $K_{b-c}(x)$ can be equivalently approximated as

$$K_{b-c}(x) = \begin{cases} \exp(-x)\sum_{n=0}^{I}\sum_{i=0}^{n}\Lambda(|b-c|,n,i)x^{i-|b-c|}, \\ \qquad \text{if} \quad b \neq c, \\ \exp(-x)\sum_{n=0}^{I}\sum_{i=0}^{n}\Lambda(2,n,i) - 2\Lambda(1,n,i)]x^{i-2}, \\ \qquad \text{if} \quad b = c, \end{cases} \quad (43)$$

where I presents the constrained upper limit of the summation, and it can be appropriately configured to meet the desired accuracy level. By applying (43), the CDFs in (12) and (13) of Theorem 1 can be approximated in compact forms as in (15) and (16) of Theorem 2, respectively.

REFERENCES

[1] T.-V. Nguyen, T. Huynh-The, and B. V.-N. Q., "Performance analysis and deep learning evaluation of URLLC full-duplex energy harvesting IoT networks over Nakagami-*m* fading channels," in *Proc. IEEE SSP Workshop*, 2023.

[2] T.-V. Nguyen, T.-N. Tran, K. Shim, T. Huynh-The, and B. An, "A deep-neural-network-based relay selection scheme in wireless-powered cognitive IoT networks," *IEEE Internet Things J.*, vol. 8, no. 9, pp. 7423–7436, May 2021.

[3] I. Parvez, A. Rahmati, I. Guvenc, A. I. Sarwat, and H. Dai, "A survey on low latency towards 5G: RAN, core network and caching solutions," *IEEE Commun. Surveys Tuts.*, vol. 20, no. 4, pp. 3098–3130, 4th Quart. 2018.

[4] W. Saad, M. Bennis, and M. Chen, "A vision of 6G wireless systems: Applications, trends, technologies, and open research problems," *IEEE Netw.*, vol. 34, no. 3, pp. 134–142, May 2019.

[5] T. Huynh-The *et al.*, "Automatic modulation classification: A deep architecture survey," *IEEE Access*, vol. 9, pp. 142 950–142 971, Oct. 2021.
[6] C. D. Ho *et al.*, "Short-packet communications in wireless-powered cognitive IoT networks: Performance analysis and deep learning evaluation," *IEEE Trans. Veh. Technol.*, vol. 70, no. 3, pp. 2894–2899, Mar. 2021.
[7] Q. Mao, F. Hu, and Q. Hao, "Deep learning for intelligent wireless networks: A comprehensive survey," *IEEE Commun. Surv. Tutor.*, vol. 20, no. 4, pp. 2595–2621, 4th Quart. 2018.
[8] T.-V. Nguyen *et al.*, "Short-packet communications in multihop networks with WET: Performance analysis and deep learning-aided optimization," *IEEE Trans. Wireless Commun.*, vol. 22, no. 1, pp. 439–456, Aug. 2022.
[9] T.-V. Nguyen, V.-D. Nguyen, D. B. da Costa, and B. An, "Short-packet communications in multi-hop WPINs: Performance analysis and deep learning design," in *Proc. IEEE GLOBECOM*, 2021.
[10] T.-V. Nguyen *et al.*, "An efficient deep CNN design for EH short-packet communications in multihop cognitive IoT networks," in *Proc. IEEE ICC*, 2022.
[11] T.-H. Vu, T.-V. Nguyen, Q.-V. Pham, D. B. da Costa, and S. Kim, "STAR-RIS-enabled short-packet NOMA systems," *IEEE Trans. Veh. Technol. (Early Access)*, May 2023.
[12] T.-H. Vu, T.-V. Nguyen, Q.-V. Pham, D. B. da Costa, and S. Kim, "Short-packet communications for UAV-based NOMA systems under imperfect CSI and SIC," *IEEE Trans. Cogn. Commun. Netw.*, vol. 9, no. 2, Apr. 2022.
[13] T.-H. Vu, T.-V. Nguyen, Q.-V. Pham, D. B. da Costa, and S. Kim, "Hybrid long-and short-packet based NOMA systems with joint power allocation and beamforming design," *IEEE Trans. Veh. Technol.*, vol. 72, no. 3, pp. 4079–4084, Mar. 2022.
[14] V. N. Q. Bao and T. T. Thanh, "Performance analysis of partial relay selection networks with short packet communications," in *Proc. IEEE NICS*, 2019.
[15] P. Raut, K. Singh, C.-P. Li, M.-S. Alouini, and W.-J. Huang, "Nonlinear EH-based UAV-assisted FD IoT networks: Infinite and finite blocklength analysis," *IEEE Internet Things J.*, vol. 8, no. 24, pp. 17 655–17 668, 2021.
[16] P. Raut, P. K. Sharma, T. A. Tsiftsis, and Y. Zou, "Power-time splitting-based non-linear energy harvesting in FD short-packet communications," *IEEE Trans. Veh. Technol.*, vol. 69, no. 8, Aug. 2020.
[17] Y. Gu, H. Chen, Y. Li, and B. Vucetic, "Ultra-reliable short-packet communications: Half-duplex or full-duplex relaying?" *IEEE Wireless Commun. Lett.*, vol. 7, no. 3, pp. 348–351, Jun. 2018.
[18] R. H. Y. Perdana, T.-V. Nguyen, and B. An, "Adaptive user pairing in multi-IRS-aided massive MIMO-NOMA networks: Spectral efficiency maximization and deep learning design," *IEEE Trans. Commun. (Early Access)*, May 2023.
[19] J. Zhang *et al.*, "Deep learning enabled optimization of downlink beamforming under per-antenna power constraints: Algorithms and experimental demonstration," *IEEE Trans. Wireless Commun.*, vol. 19, no. 6, pp. 3738–3752, Jun. 2020.
[20] L. J. Rodriguez, N. H. Tran, and T. Le-Ngoc, "Performance of full-duplex AF relaying in the presence of residual self-interference," *IEEE J. Sel. Areas Commun.*, vol. 32, no. 9, pp. 1752–1764, Sep. 2014.
[21] M. Mohammadi, B. K. Chalise, H. A. Suraweera, H. Q. Ngo, and Z. Ding, "Design and analysis of full-duplex massive antenna array systems based on wireless power transfer," *IEEE Trans. Commun.*, vol. 69, no. 2, pp. 1302–1316, Feb. 2021.
[22] A. A. Nasir, H. D. Tuan, H. Q. Ngo, T. Q. Duong, and H. V. Poor, "Cell-free massive MIMO in the short blocklength regime for URLLC," *IEEE Trans. Wireless Commun.*, vol. 20, no. 9, pp. 5861–5871, 2021.
[23] T. Riihonen, S. Werner, and R. Wichman, "Mitigation of loopback self-interference in full-duplex mimo relays," *IEEE Trans. Signal Process.*, vol. 59, no. 12, pp. 5983–5993, Aug. 2011.
[24] I. Shomorony and A. S. Avestimehr, "Is gaussian noise the worst-case additive noise in wireless networks?" in *Proc. IEEE ISIT*, 2012.
[25] S. Sohaib and M. Uppal, "Full-duplex compress-and-forward relaying under residual self-interference," *IEEE Trans. Veh. Technol.*, vol. 67, no. 3, pp. 2776–2780, Apr. 2017.
[26] Y. Ni, H. Zhao, Y. Liu, J. Wang, G. Gui, and H. Zhang, "Analysis of RIS-aided communications over Nakagami-m fading channels," *IEEE Trans. Veh. Technol.*, no. 7, pp. 8709–8721, Feb. 2023.
[27] T. Huynh-The, C.-H. Hua, Q.-V. Pham, and D.-S. Kim, "MCNet: An efficient CNN architecture for robust automatic modulation classification," *IEEE Commun, Lett.*, vol. 24, no. 4, pp. 811–815, Apr. 2020.
[28] K. He, X. Zhang, S. Ren, and J. Sun, "Deep residual learning for image recognition," in *Proc. IEEE CVPR*, 2016.
[29] T. Huynh-The, T.-V. Nguyen, Q.-V. Pham, D. B. da Costa, and D.-S. Kim, "MIMO-OFDM modulation classification using three-dimensional convolutional network," *IEEE Trans. Veh. Technol.*, vol. 71, no. 6, pp. 6738–6743, Mar. 2022.
[30] O. L. A. López, H. Alves, R. D. Souza, and E. M. G. Fernández, "Ultrareliable short-packet communications with wireless energy transfer," *IEEE Signal Process. Lett.*, vol. 24, no. 4, pp. 387–391, Apr. 2017.
[31] I. S. Gradshteyn and I. M. Ryzhik, *Table of integrals, series, and products*. Academic Press, 2007.

Toan-Van Nguyen (Member, IEEE) received the B.S. degree in Electronics and Telecommunications Technology and the M.Eng. degree in Electronic Engineering from HCMC University of Technology and Education, Vietnam, in 2011 and 2014, respectively, and the Ph.D. degree in Electronics and Computer Engineering from Hongik University, South Korea, in 2021. He is currently a Postdoctoral Researcher in the Department of Electrical and Computer Engineering at San Diego State University, CA 92182, USA. His current research activity is focused on the mathematical modeling of beyond 5G networks, and machine learning for wireless communications.

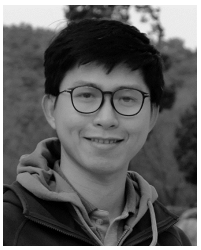

Thien Huynh-The (Senior Member, IEEE) received the B.S. degree in Electronics and Telecommunication Engineering and the M.Sc. degree in Electronics Engineering from Ho Chi Minh City University of Technology and Education (HCMUTE), Vietnam, in 2011 and 2013, respectively and the Ph.D. degree in Computer Science and Engineering from Kyung Hee University (KHU), South Korea, in 2018. He was a recipient of the Superior Thesis Prize awarded by KHU. From March 2018 to August 2018, he was a Postdoctoral Researcher with Ubiquitous Computing Laboratory, KHU. From September 2018 to May 2022, he was a Postdoctoral Researcher with ICT Convergence Research Center, Kumoh National Institute of Technology, South Korea. He is currently a Lecturer in Department of Computer and Communications Engineering, HCMUTE, Vietnam. He was a recipient of Golden Globe Award 2020 for Vietnamese Young Scientist by Central Ho Chi Minh Communist Youth Union associated with Ministry of Science and Technology. His current research interests include digital image processing, radio signal processing, computer vision, wireless communications, IoT applications, machine learning, and deep learning.

Vo-Nguyen Quoc Bao (Senior Member, IEEE) (M'11—SM'16) served as the Dean of the Faculty of Telecommunications and the Director of the Wireless Communication Laboratory. He is currently a Professor of Wireless Communications with the Posts and Telecommunications Institute of Technology, Vietnam. He has authored over 200 journal and conference articles that have over 3800 citations and H-index of 30. His research interests include wireless communications and information theory with current emphasis on MIMO systems, cooperative and cognitive communications, physical layer security, and energy harvesting. He is a member of the Executive Board of the Radio-Electronics Association of Vietnam and the Electronics Information and Communications Association Ho Chi Minh City. He served as the Technical Program Co-Chair of ATC (2013 and 2014), NAFOSTED, NICS (2014, 2015, and 2016), REV-ECIT 2015, ComManTel (2014 and 2015), and SigTelCom 2017. He is currently serving as a Scientific Secretary of the Vietnam National Foundation for Science and Technology Development Scientific Committee in Information Technology and Computer Science. He is a Technical Editor-in-Chief of REV Journal on Electronics and Communications since 2017, an Associate Editor of the EURASIP Journal on Wireless Communications and Networking, an Editor of the Transactions on Emerging Telecommunications Technologies (Wiley ETT), the VNU Journal of Computer Science and Communication Engineering, and the REV Journal on Electronics and Communications. Mr. Bao's awards and honors include IEEE Exemplary Reviewer for IEEE Wireless Communications in 2013, best paper award at the 9th International Conference on Communications and Networking in China (ChinaCom) in 2014, Best Paper Award at the International Conference on Computing, Management and Telecommunications (ComManTel) in 2013, and outstanding paper award at the 14th International Conference on Advanced Communication Technology (ICACT) in 2012.